Photoactivated Chemotherapy Agents

Photolabile Ru Model Complexes with Chelating Diimine Ligands for Light-Triggered Drug Release

Federica Battistin,[a] Gabriele Balducci,[a] Jianhua Wei,[b] Anna K. Renfrew,*[b] and Enzo Alessio*[a]

Abstract: A series of water-soluble photolabile model complexes of the general formula $[Ru([9]aneS_3)(chel)(py)]Cl_2$ ([9]aneS$_3$ = 1,4,7-trithiacyclononane, chel = chelating diimine) was prepared and fully characterized. The phototriggered release of pyridine with visible light as a function of the nature of the diimine {chel = 2,2′-bipyridine (**6**) 1,10-phenanthroline (**7**), 4,7-diphenil-1,10-phenanthroline (**8**), dipyrido-[3,2-*a*:2′,3′-*c*]-phenazine (dppz, **9**), 2,2′-biquinoline (bq, **10**)} was investigated. Our aim is to establish whether this type of complexes might be realistically used in the photo-uncaging strategy of photoactivated chemotherapy (PACT) in the future. Compounds **6**–**9** present a MLCT absorption in the blue region of the visible spectrum. When irradiated with light at 470 nm, they rapidly and quantitatively release the coordinated pyridine. Complex **10** turned out to be quite different from the others in the series. Structure-wise, in **10** the average plane of coordinated bq – owing to its steric demand – is remarkably tilted relative to the equatorial coordination plane [37.43(4)°, with the "front" of the ligand pointing towards the axial py] and the orientation of py is nearly orthogonal compared to that found in **6** and **7** for minimizing steric clashes with bq. The low-lying acceptor orbitals of bq induce a red-shift of the MLCT absorption maximum to ca. 500 nm. Contrary to the expectations, complex **10** is more photostable compared to **6**–**9** and photo-dissociation of both py and bq, in nearly equal amounts, occurs. A detailed theoretical investigation was performed on **10** (and on **6** for comparison), for explaining its peculiar spectral features and photochemical behavior.

1. Introduction

In therapy, light-triggered treatments are appealing since – in principle – they can generate a drug with high spatial and temporal selectivity, resulting in a greater specificity of action. Such treatments require light-activated prodrugs that – ideally – are inactive and non-toxic in the dark, whereas they are locally activated in vivo upon irradiation with visible light. In this context, photodynamic therapy (PDT), a clinically approved treatment for some skin diseases, age-related macular degeneration and some cancers, is the most well-known application. PDT uses a photosensitizer (PS) at non-toxic concentrations that, in the most common type II mechanism, upon light-excitation catalytically generates singlet oxygen ($^1O_2$) or other highly cytotoxic ROS such as superoxide radical anions.[1] Another phototherapy approach is the so-called photoactivated chemotherapy (PACT) in which a kinetically inert and biologically non-active prodrug is irreversibly activated by irradiation with visible light that induces the cleavage of a photolabile protecting group.[2] The photoactivation process is also called photo-uncaging. Compared to PDT, PACT is a stoichiometric rather than catalytic process, but has the advantage of not depending on the presence of molecular oxygen. Thus, in principle, PACT agents are active also in hypoxic tumor tissues. In general, ideal PDT or PACT agents are water-soluble and resistant to photobleaching. In addition, they should be activated within the phototherapeutic window ($\lambda > 600$ nm), where light is more penetrating into the tissues and less harmful.

By virtue of their peculiar light absorption properties and rich photoreactivity, d-block metal compounds are attracting rapidly increasing interest as potential PDT and PACT agents.[3–7] Among them, Ru^{II} compounds are extensively investigated due to their superior photophysical and photochemical properties.[8–10] For example, even though most PDT photosensitizers used in clinic are based on porphyrin derivatives,[11] a Ru^{II}-polypyridyl complex (TLD-1433) is undergoing a phase I clinical trial in Canada as PDT agent in patients with bladder cancer.[12,13]

A typical reaction that can occur in inorganic PACT agents is the photoinduced release of ligands from coordinatively saturated and inert prodrugs. The most extensively investigated class of ruthenium PACT agents is that of polypyridyl complexes of the $[Ru(bpy)_3]^{2+}$ family that contain (at least) one sterically hindering diimine such as 6,6′-dimethyl-2,2′-bipyridine (dmbpy).[14] The strain caused by such a ligand in the coordination sphere promotes the light-induced population of low-lying

[a] *Department of Chemical and Pharmaceutical Sciences, University of Trieste, Via L. Giorgieri 1, 34127 Trieste, Italy*
E-mail: alessi@units.it
http://dscf.units.it/en/department/people/alessio-enzo/1055
[b] *School of Chemistry, University of Sydney, Sydney, NSW, 2006, Australia*
E-mail: anna.renfrew@sydney.edu.au
http://sydney.edu.au/science/people/anna.renfrew.php

dissociative metal-centered triplet excited states (^{3}MC) and consequently its release. Coordination and organometallic Ru^{II} compounds in which visible light triggers the release of a single monodentate ligand have also been investigated.[15,16] A careful design of the metal prodrug can lead to metal complexes with dual activity, i.e. phototriggered ligand release (PACT) and singlet oxygen production (PDT).[17] The activation of coordinatively saturated cytotoxic Ru complexes through the photodeprotection of a ligand has also been reported.[18]

In photolabile metal complexes the focus can be on the activated metal fragment that may bind to biomolecules such as DNA through its newly generated coordination sites,[14,19] or on the released ligand if it is itself a pharmacologically active molecule,[20] or on the combined action of both.[21] In polypyridyl Ru^{II} complexes the increased cytotoxicity is generally attributed to the intracellular formation of the bis(aqua) complex *cis*-$[Ru(bpy)_2(OH_2)_2]^{2+}$ species. However, a very recent paper by Bonnet and co-workers demonstrated that in the case of $[Ru(bpy)_2(dmbpy)]^{2+}$ the photoreleased dmbpy ligand, rather than the ruthenium bis(aqua) fragment, is responsible for the observed phototoxicity.[22]

In the recent past we reported that dicationic Ru^{II} complexes, such as $[Ru([9]aneS_3)(bpy)(py)][PF_6]_2$ ([9]aneS$_3$ = 1,4,7-trithiacyclononane, bpy = 2,2′-bipyridine), are inert in the dark but rapidly and quantitatively release the pyridine ligand in aqueous solution when illuminated with blue light (λ = 420 nm).[23,24] Since the photogenerated aqua species $[Ru([9]aneS_3)(bpy)(OH_2)]^{2+}$ showed a substantial lack of cytotoxicity (against the MDA-MB-231 human mammary carcinoma cell line) we suggested that Ru^{II} compounds of this type might be suitable PACT agents for the light-triggered release of coordinated drugs (*photo-uncaging*).[25]

In this paper we report our recent work on the model complexes of the type $[Ru([9]aneS_3)(chel)(py)]Cl_2$, where chel is a chelating diimine. Our aim was to establish whether complexes of this series, bearing a pharmacologically active molecule in the place of pyridine, can be realistically used within the photo-uncaging strategy. First we investigated whether the absorption maxima in the visible spectrum and the photoinduced release of pyridine could be tuned by changing the nature of the diimine ligand. For this purpose, the model complexes with chel = 1,10-phenanthroline (phen), 4,7-diphenil-1,10-phenanthroline (4,7-Ph$_2$phen), dipyrido-[3,2-*a*:2′,3′-*c*]phenazine (dppz), 2,2′-biquinoline (bq) were prepared, fully characterized and investigated. The photoinduced release of py was qualitatively investigated by ^{1}H NMR and UV/Vis spectroscopy. A particularly detailed experimental and theoretical investigation was performed on the bq derivative, for explaining its peculiar spectral features and photochemical behavior.

2. Results and Discussion

2.1. Diimine Ligands

The chelating diimines used in this work, with different size and aromaticity, are shown in Figure 1. The 2,2′-biquinoline ligand, owing to its steric demand, is known to induce deformation in the pseudo-octahedral coordination sphere of Ru^{II} complexes that can improve the photoinduced dissociation of ligands.[14b,15] In addition, its low-lying acceptor orbitals are expected to red-shift the ^{1}MLCT absorption maximum typical of diimine-Ru^{II} complexes closer to the PDT window.[26,27]

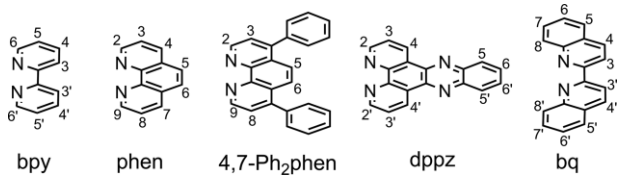

Figure 1. The diimine ligands used in this work with proton labelling scheme for NMR purposes: 2,2′-bipyridine (bpy), 1,10-phenanthroline (phen), 4,7-diphenil-1,10-phenanthroline (4,7-Ph$_2$phen), dipyrido-[3,2-*a*:2′,3′-*c*]phenazine (dppz), 2,2′-biquinoline (bq).

2.2. Synthesis of the Complexes

The Ru^{II} compounds were prepared as chloride salts, rather than as PF_6 salts, for improving aqueous solubility. A two-step procedure was followed (Scheme 1).

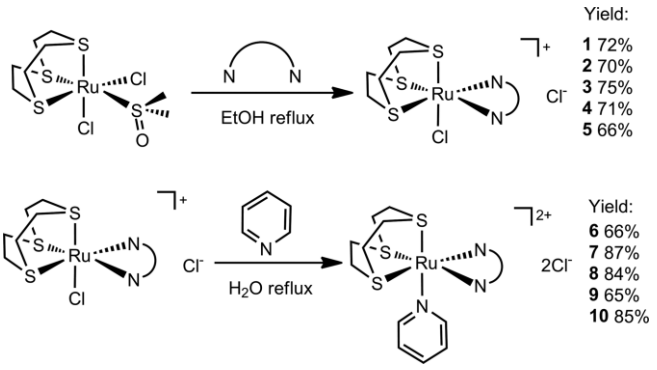

Scheme 1. Synthetic procedure for the $[Ru([9]aneS_3)(chel)(py)]Cl_2$ compounds **6**–**10**, chel = bpy (**6**), phen (**7**), 4,7-Ph$_2$phen (**8**), dppz (**9**), bq (**10**).

In the first step, modified from the literature,[28] treatment of the $[Ru([9]aneS_3)(dmso\text{-}S)Cl_2]$ precursor with a twofold excess of chel in refluxing ethanol (3 h) afforded the known monocationic intermediates of formula $[Ru([9]aneS_3)(chel)Cl]Cl$ {chel = bpy (**1**), phen (**2**), 4,7-Ph$_2$phen (**3**), dppz (**4**)} in good isolated yields (65–85 %). The insertion of bq was more difficult, possibly due also to the low solubility of the ligand in ethanol. A microwave assisted reaction in ethanol (140 °C, 90 min) was preferred to prolonged reflux for obtaining $[Ru([9]aneS_3)(bq)Cl]Cl$ (**5**) in good yield. All complexes, already reported in the literature either as Cl or PF_6 salts,[28,29] were characterized by NMR and UV/Vis spectroscopy (Supporting Information, Figure S1), and mass spectrometry. They are well soluble in ethanol, chloroform, DMSO, and – with the exception of **3** and **4** – also in water.

As clearly shown by ^{1}H NMR spectroscopy (Figure S2), in D_2O compounds **1**–**5** are in equilibrium – to different extents – with the corresponding aqua species $[Ru([9]aneS_3)(chel)(OH_2)]^{2+}$ (**1aq** – **5aq**). In **1aq**–**4aq** the aromatic resonances are slightly downfield shifted (ca. 0.1 pm or less) compared to those of

the parent complex, and their relative intensity increases upon diluting the solution and decreases (or disappears altogether) upon adding an excess of NaCl. In the case of **5** a single set of resonances is observed in D_2O, suggesting that no significant equilibration with the aqua species **5aq** occurs at typical NMR concentrations. The resonances of **5aq** appear upon dilution, and in this case some of them are shifted upfield compared to those of **5** (e.g. the doublet of H8,8′ falls at δ = 9.26 ppm in **5** and at δ = 9.09 ppm in **5aq**). The resonances of $[Ru([9]aneS_3)(dppz)Cl]^+$ (**4**), that are sharp in $CDCl_3$, are rather broad and have concentration-dependent shifts in D_2O, most likely due to stacking interactions occurring in solution. Consistent with this hypothesis, they (and those of **4aq** as well) become sharper upon diluting the solution.

Treatment of intermediates **1**–**5** with a slight excess of pyridine in refluxing water afforded the corresponding dicationic complexes $[Ru([9]aneS_3)(chel)(py)]Cl_2$ {chel = bpy (**6**), phen (**7**), 4,7-Ph_2phen (**8**), dppz (**9**), bq (**10**)} that, with the exception of **6** previously reported by us as PF_6 salt,[23] are described here for the first time. They were fully characterized as **1**–**5** above, and the single-crystal X-ray structures of **7** (Figure S3) and **10** (Figure 2) were also determined. In **10**, as in its precursor **5** and other bq octahedral complexes,[14b,15,28–30] the distortion in the geometry induced by the sterically demanding diimine is evident. In particular, the average plane of bq is remarkably tilted relative to the equatorial coordination plane [37.43(4)°, with the "front" of the ligand pointing towards the axial py], whereas the twist about the C–C bond between the two quinolines [3.9(2)°] is negligible. The geometrical features of coordinated bq are similar also in the *trans*-$RuCl_2(bq)(CO)_2$ (**11**) complex (Figure 2), in which the other ligands are sterically undemanding and that we expressly prepared for the sake of comparison. Another major structural difference in **10** concerns the rotation of the py ligand about the Ru–N bond: in **10** py is nearly orthogonal compared to the other similar complexes (e.g. ca. 76° with respect to complex **6**), most likely for avoiding steric clashes between the *o*H atoms of py and H8,8′ of bq.

All dicationic complexes are fairly soluble in water. The ^{1}H NMR spectra of compounds **6**–**9** (Figures S4 – S7) are unexceptional and, as for the corresponding precursors, consistent with the C_S symmetry of each complex cation. The most downfield resonance is that of the protons adjacent to the N atoms of the diimine ligand. The ^{1}H NMR spectrum of the bq compound **10** is treated in more detail below.

The electronic absorption spectra of **6**–**9** in the visible region are characterized by two bands of roughly comparable intensities (ε in the range 3000–6000 M^{-1} cm^{-1}), partially or completely overlapped, at 350–430 nm. The spectrum of **10**, instead, shows two rather sharp and more intense bands at 359 and 378 nm, whereas the lowest energy MLCT band – in good agreement with the expectations – is red-shifted, with an absorption maximum at nearly 500 nm (Figure 3).

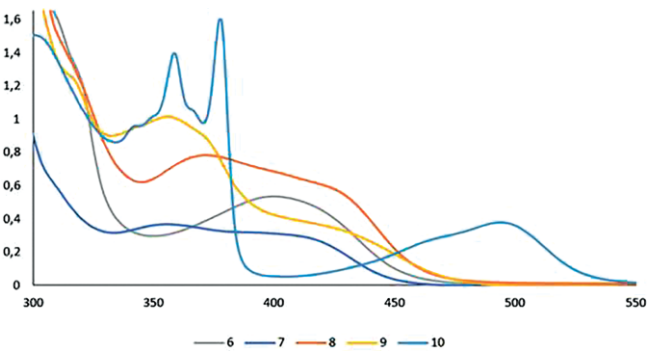

Figure 3. UV/Vis spectra in the visible region of compounds **6**–**10** (ca. in 0.1 mM H_2O).

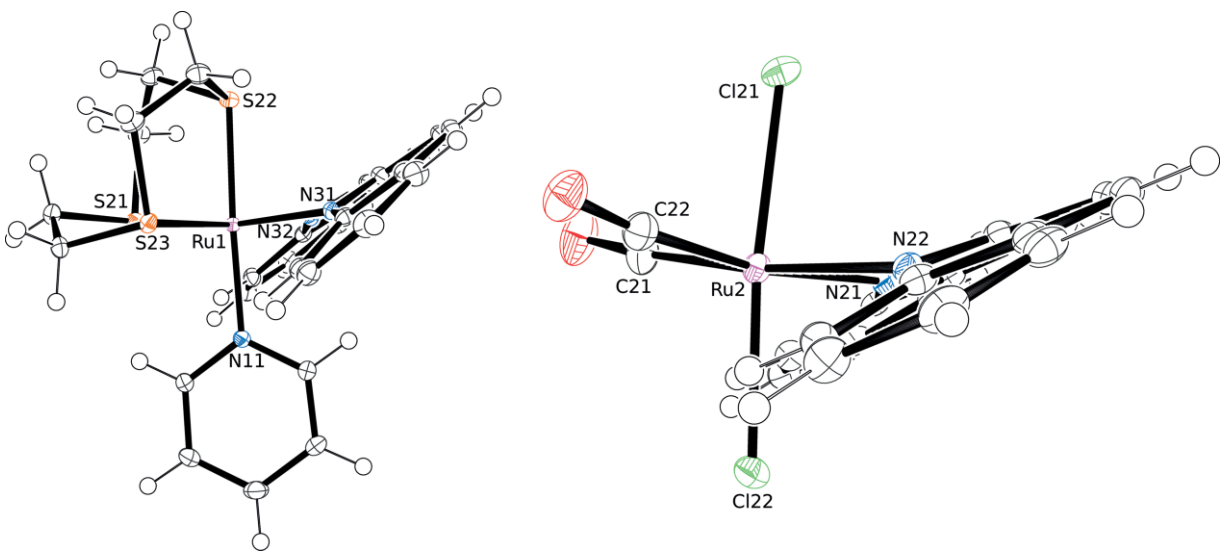

Figure 2. X-ray molecular structures (50 % probability ellipsoids) of $[Ru([9]aneS_3)(bq)(py)]Cl_2$ (**10**) (left) and of *trans*-$RuCl_2(bq)(CO)_2$ (**11**) (right). The two chlorides in **10**, and two chloroform crystallization molecules in **11** omitted for clarity. Only one of the two independent molecules of **11** present in the unit cell is shown.

2.3. The 2,2′-Biquinoline Complexes

In the ^{1}H NMR spectrum of 2,2′-biquinoline the most downfield resonance is that of H3,3′, followed by that of H4,4′. The *anti* conformation assumed by the two quinolines in the free ligand brings N′ close to H3 (and N to H3′), and the deshielding of H3,3′ was attributed mainly to the electrostatic effect of the lone pairs (Figure 4).[31] When symmetrically bound to diamagnetic octahedral metal centers, such as in $Re(CO)_3(bq)Br$,[32] the proton NMR spectrum of bq undergoes remarkable changes: the doublet of H8,8′ becomes the most downfield signal ($\Delta\delta$ = 0.71 ppm), whereas that of H3,3′ is shifted to lower frequencies ($\Delta\delta$ = –0.50 *ppm*). Such variations are attributable to the conformational change of the ligand (from *anti* to *syn*) and to its coordination. Regretfully, in the other symmetrical Ru-bq compounds such as $[Ru(phen)_2(bq)][PF_6]_2$,[14b] $[Ru(\eta^6\text{-p-cymene})(bq)Cl][PF_6]$,[33] and $[Ru(bq)_3][PF_6]_3$,[34] the proton NMR spectra were not assigned.

We found that, whereas the ^{1}H NMR spectrum of **5** is consistent with such features, the spectrum of **10** is quite different and more similar to that of the free ligand: the resonance of H8,8′ falls to lower frequencies than those of H3,3′ and H4,4′ (Figure 4).

Since these changes in the chemical shifts of the bq protons between **5** and **10** could not be attributed to different conformational strains in the bq frame (see above), we came to the conclusion that the H8,8′ doublet in **10** is shifted upfield by the shielding cone of the adjacent axial pyridine. In order to confirm this hypothesis, that is consistent also with the orientation of py evidenced by the X-ray structure shown in Figure 2, we prepared the complex with NH_3 in the place of pyridine, i.e. $[Ru([9]aneS_3)(bq)(NH_3)]Cl_2$ (**12**). Indeed, even though the structural features in **12** (Figure 5) are again similar to those of **5** and **10** [e.g. the tilt angle of bq is 38.89(3)°], the NMR spectral pattern of coordinated bq follows the "normal" order, and the H8,8′ doublet is again the most downfield resonance.[35]

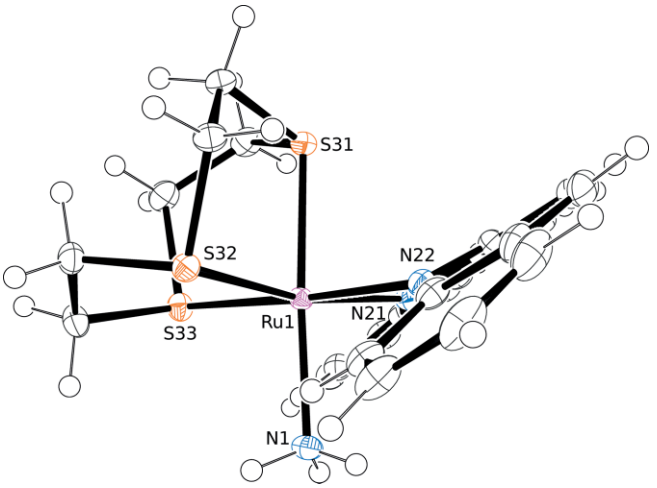

Figure 5. X-ray molecular structure (50 % probability ellipsoids) of $[Ru([9]aneS_3)(bq)(NH_3)]Cl_2$ (**12**). The two chlorides and a methanol crystallization molecule omitted for clarity.

2.4. Photoinduced Release of Ligands

In the dark, compounds **6**–**10** are stable in D_2O (3 mM solutions) for at least 24 h at ambient temperature, no changes in the NMR spectra were observed.

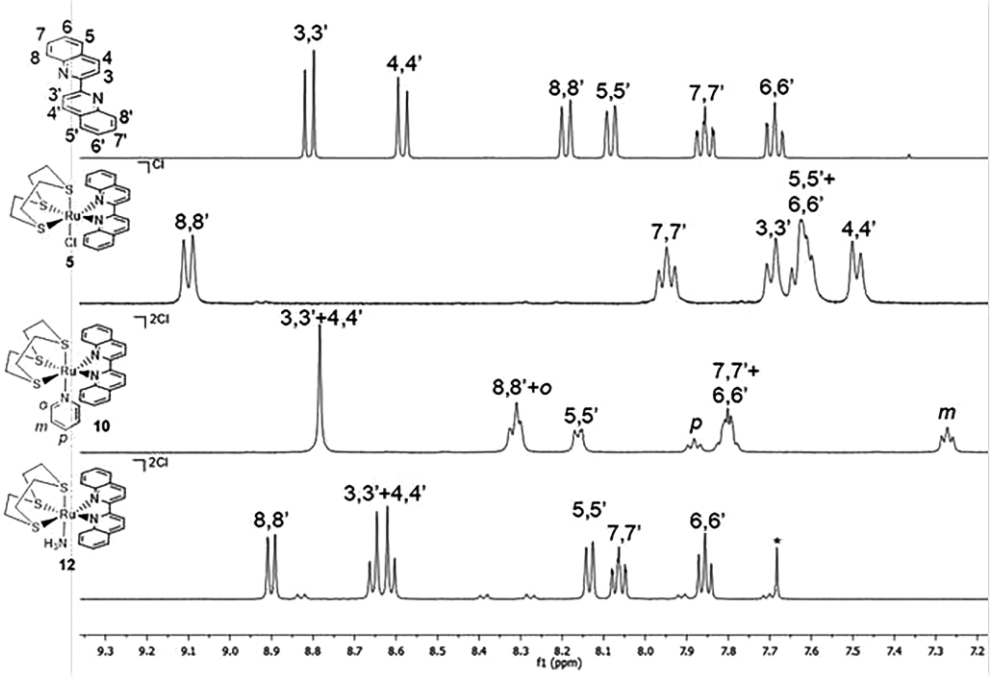

Figure 4. ^{1}H NMR spectrum (aromatic region) of, from top to bottom: 2,2′-biquinoline, $[Ru([9]aneS_3)(bq)Cl]Cl$ (**5**), $[Ru([9]aneS_3)(bq)(py)]Cl_2$ (**10**), and $[Ru([9]aneS_3)(bq)(NH_3)]Cl_2$ (**12**). The spectrum of bq is in $[D_6]$DMSO, the others in D_2O. In the spectrum of **12** the asterisk indicates residual chloroform.

Form our previous work it is already known that, when irradiated with blue light at 420 nm, $[Ru([9]aneS_3)(bpy)(py)][PF_6]_2$ rapidly and quantitatively releases the coordinated pyridine.[23]

Compounds **6**–**9** have a similar behavior: when irradiated with blue light (LED, λ = 470 nm, 40 mW) they release the coordinated pyridine at comparable rates and extents, generating selectively the corresponding aqua species (**1aq**–**4aq**) in equilibrium with the chlorido species (**1**–**4**) (Scheme 2). No other reaction occurs.

The photoreactions were performed in D_2O and quantitatively monitored by ^1H NMR spectroscopy. An example is reported in Figure 6. In the case of the dppz complex **9**, the resonances of the photogenerated aqua and chlorido species – as mentioned above – are rather broad; the sharp pyridine signals allowed reliable integration to be performed. Table 1 reports the percentage amount of photoreleased pyridine as a function of the irradiation time.

Table 1. Extent of photoreleased pyridine, assessed by ^1H NMR spectroscopy, as a function of the irradiation time (LED, λ = 470 nm, 40 mW).

Complex (ligand)	5 min	10 min	15 min	30 min
6 (bpy)	80,0 %	92,8 %	93.3 %	98.8 %
7 (phen)	60.0 %	78.2 %	87.8 %	96.6 %
8 (4,7-Ph_2phen)	75.0 %	78.8 %	81.4 %	95.4 %
9 (dppz)	50.0 %	75.0 %	85.0 %	97.7 %

In summary, the photo-dissociation of py is almost complete after 30 min of illumination and the bpy complex **6** is the fastest one, even though it has the smallest absorption coefficient at 470 nm. We found that the dppz complex **9**, that has a very weak absorption at ca. 540 nm (Figure S8), is still photoactive when irradiated with green light at 530 nm, even though the photorelease of pyridine is slower: 33 % after 15 min (λ = 530 nm, 30 mW) compared to 78 % when irradiation was performed at 470 nm with the same power.

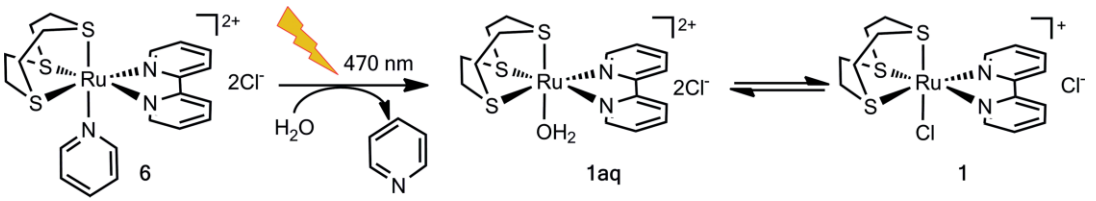

Scheme 2. Photo-dissociation of pyridine from compounds **6**–**9**, exemplified in the case of chel = bpy.

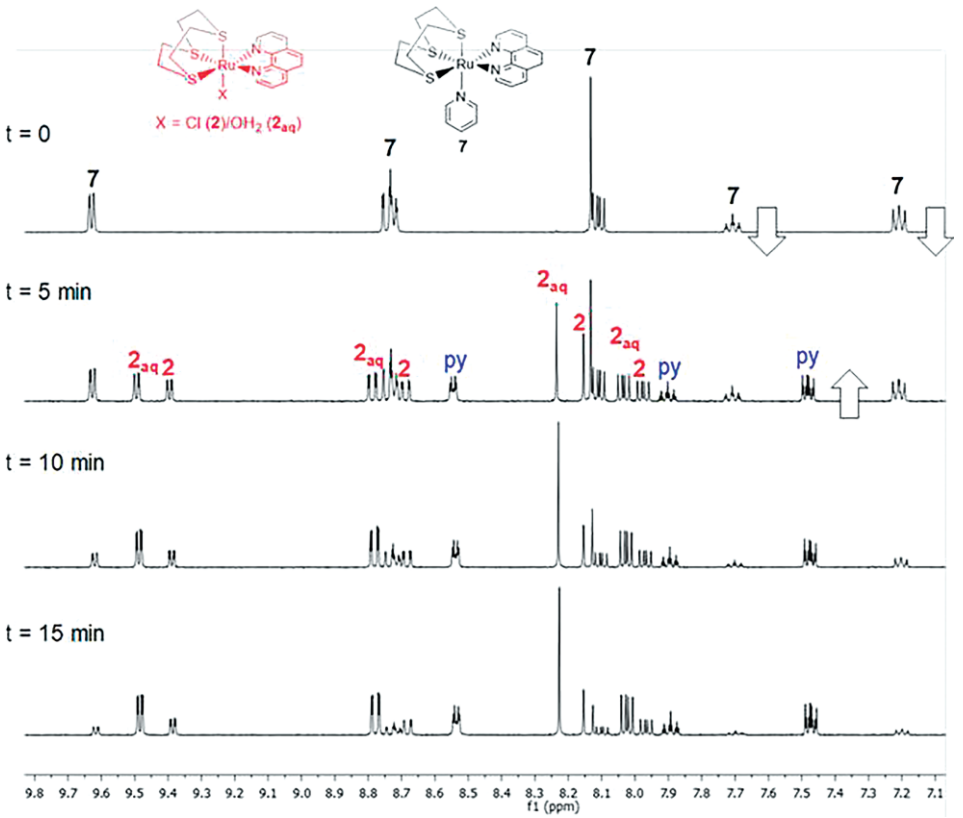

Figure 6. Photoinduced dissociation of pyridine from $[Ru([9]aneS_3)(phen)(py)]Cl_2$ (**7**) monitored as a function of the irradiation time (λ = 470 nm, 40 mW) by ^1H NMR spectroscopy in D_2O. The positive charges of the complexes are omitted.

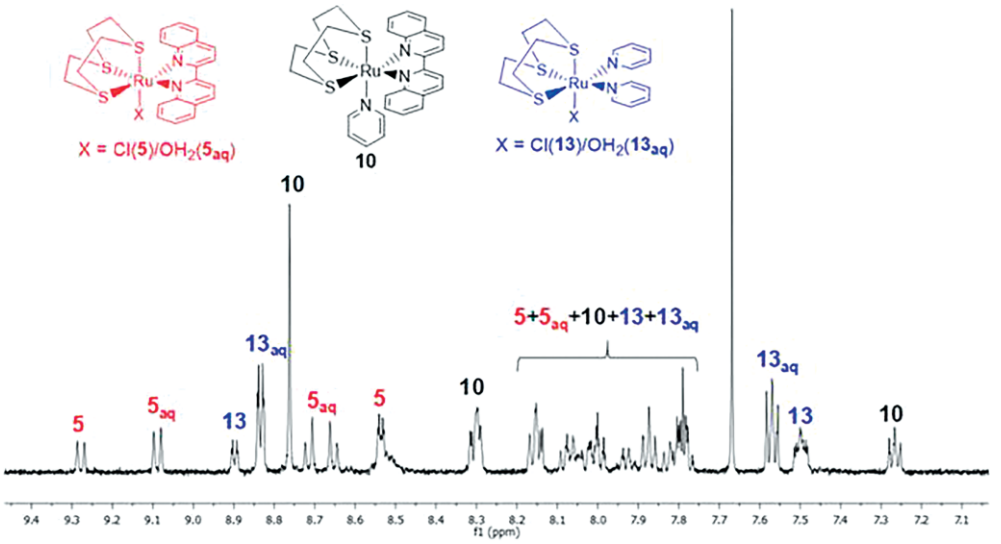

Figure 7. ^{1}H NMR spectrum of the reaction mixture obtained upon irradiation (λ = 470 nm, 40 mW, 180 min) of a D_2O solution of [Ru([9]aneS$_3$)(bq)(py)]Cl$_2$ (**10**). The positive charges of the complexes are omitted.

The behavior of the bq complex **10** upon illumination is quite different, and photo-dissociation of both py and bq in nearly equal amounts occurs. In general, contrary to the expectations, the complex is more photostable compared to **6**–**9**: after 2 h of illumination at 470 nm (40 mW) in D_2O ca. 25 % of **10** is still present in solution. The interpretation of the NMR spectra (Figure 7) was made more difficult by the following facts: (1) 2,2′-biquinoline is insoluble in water, thus the resonances of photoreleased bq cannot be seen; (2) the chemical shifts of the bq resonances in both **5** and **5aq**, i.e. the Ru complexes obtained upon photorelease of py, as well as the ratio between the two species, are concentration-dependent; (3) (most of) the released py binds to the {Ru([9]aneS$_3$)(py)}$^{2+}$ fragment (thus the resonances of free py are not clearly seen), affording the [Ru([9]aneS$_3$)(py)$_2$(OH$_2$)]$^{2+}$ complex cation that, in addition, is in equilibrium with [Ru([9]aneS$_3$)(py)$_2$Cl]$^+$. The resonances of these latter species were unambiguously identified: for this purpose we made [Ru(9aneS3)(py)$_2$Cl]Cl (**13**), that in aqueous solution equilibrates with [Ru([9]aneS$_3$)(py)$_2$(OH$_2$)]$^{2+}$ (**13aq**). When a D_2O solution of **10** was irradiated with green light (30 mW) at 530 nm a similar behavior was observed, but the photorelease of both bq and py was slower. A similar photochemistry was observed when the irradiation of **10** was performed in [D$_6$]DMSO where the resonances of free bq (that is soluble) could be observed: in this medium the photoinduced dissociation of bq prevails over that of py (Figure S9).

Although parallel photorelease of two different ligands has not been often described, it has been observed recently in the complex [Ru(bpy)(dmbpy)(L-proline)][PF$_6$], in which substitution of both dmbpy and L-proline occurred upon illumination.[36]

2.5. Theoretical Calculations

Intrigued by the remarkably different photochemical behavior of the biquinoline complex **10**, we performed a series of theoretical calculations on it and on the corresponding bpy complex **6**, taken as model for the other diimine compounds **7**–**9**. Structure-wise, complex **10** has two main geometrical differences compared to the canonical features of **6**, which are likely to be related to its different photochemistry: the tilted geometry of bq and the orientation of py (see above).

First of all, our computational protocol (DFT with plane wave basis set, pseudopotentials and periodic boundary conditions) was tested on compound **6** that had been previously investigated using a different computational approach (DFT with localized basis functions).[23] The results obtained in terms of optimized geometry, calculated MOs, and electronic transitions were in excellent agreement with those reported in the literature, thus confirming the reliability of our protocol. Next, the calculations were extended to **10**.

Figure 8 shows the density of states and its projection onto selected atomic orbitals of the Ru, py and bq or bpy ligands for complexes **10** and **6** in the ground state configuration.

Consistent with the red-shifted absorption band in the UV/Vis spectrum, and with the general features expected for bq complexes (i.e. stabilized bq π^* orbitals relative to those of bpy),[14b,15] the HOMO–LUMO energy gap in **10** is smaller than that in **6** (2.01 vs. 2.32 eV). TDDFT calculations well reproduced the experimental absorption spectrum of both complexes (Figures 9 and S10) and allowed us to assign also the character of each band (Table S1),[37] thus confirming that the lowest energy transition has a ca. 85–90 % HOMO $\rightarrow$ LUMO component.[23] In both complexes the LUMO is almost coincident with a π^* MO of the diimine ligand (Figure S11). However, we notice that whereas in the bpy complex the three frontier occupied orbitals – HOMO, HOMO–1 and HOMO–2 (Figure S11) – have an almost exclusive metal-centered character, i.e. are coincident with the filled d orbitals of Ru^{II}, in **10** the HOMO and HOMO–1 get an appreciable contribution from the atomic orbitals of C and N atoms of the biquinoline ligand (see also Figure 8). We argue that the tilted orientation of bq in **10** is responsible for the mixing of diimine π orbitals with the filled d orbitals of Ru^{II}.

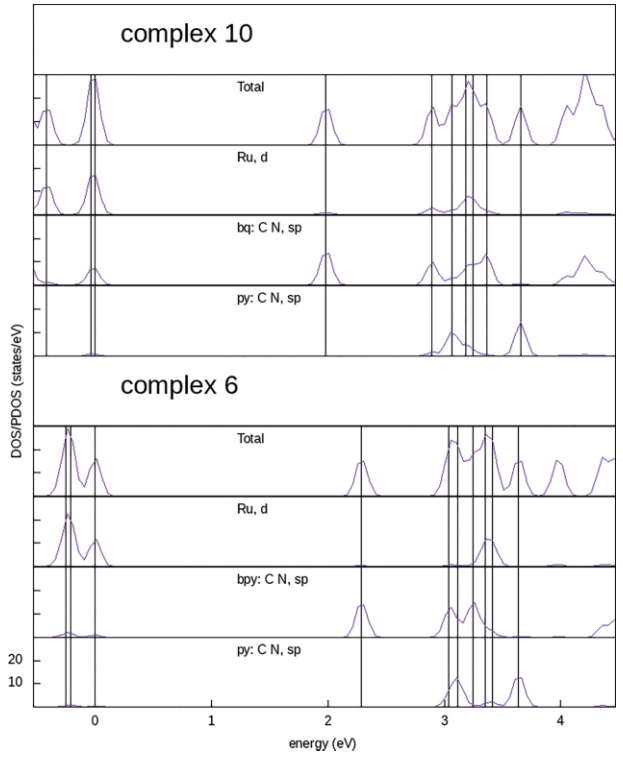

Figure 8. Density of states (DOS) and its projection onto selected atomic orbitals for complexes **10** (top) and **6** (bottom). Vertical lines indicate the energy of the molecular orbitals in the range from HOMO–2 to LUMO+6. Plots have been aligned so that the energy of the HOMOs for the two complexes is 0.0 eV.

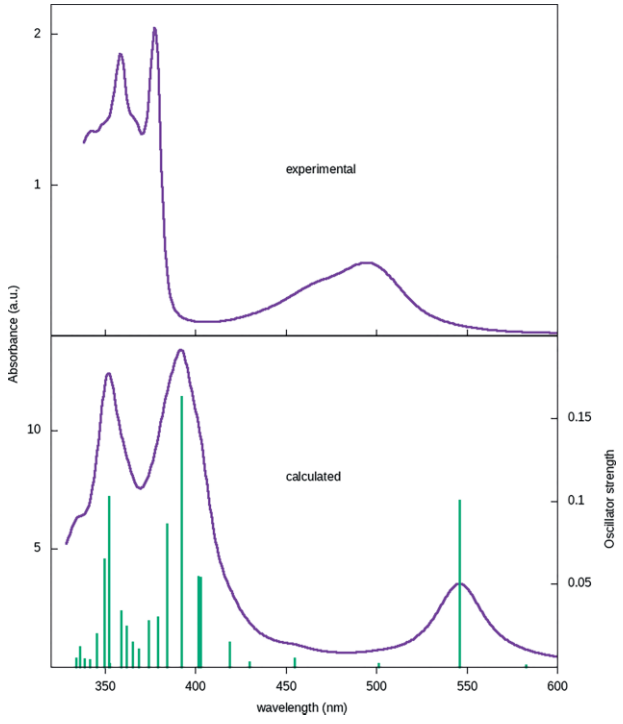

Figure 9. Experimental (top) and calculated (with the "turbo_lanczos" program, bottom) absorption spectra for complex **10**. The vertical bars in the simulated spectrum are the calculated transitions (with the "turbo_davidson" code), with height equal to the oscillator strength.

Therefore, the lowest energy electronic transition can be safely labeled as a pure MLCT in **6**, whereas it has a π–π*component in **10**.

Consistent with what previously observed, in **6** the LUMO+4 and LUMO+5 MOs have a strong metal d-antibonding component; in addition, they have a significant σ-antibonding character towards the bpy and – above all – the pyridine ligands (Figure 10). Thus, the light-induced population of such orbitals is presumably responsible for the photo-dissociation of py. Conversely, in **10** the orbitals with the most relevant d* component are the LUMO+3 and LUMO+4, and they have a relevant bq – rather than py – contribution (Figure 10). This finding is consistent with what established for Ru^{II}-polypyridyl complexes that contain bq, in which distortion is known to lower the energy of a dissociative metal-centered state.[14b,15] In addition, whereas LUMO+4 has a significant σ-antibonding character towards bq, in both the LUMO+3 and LUMO+4 the antibonding character towards py is mainly of π symmetry (i.e. involving p atomic orbitals normal to the py plane). This finding, i.e. the increase of π back-bonding from the filled metal orbital to the π* orbitals of py, is most likely attributable to the different orientation of py in the bq complex and might account for the less-pronounced light-induced dissociation of pyridine in **10**.

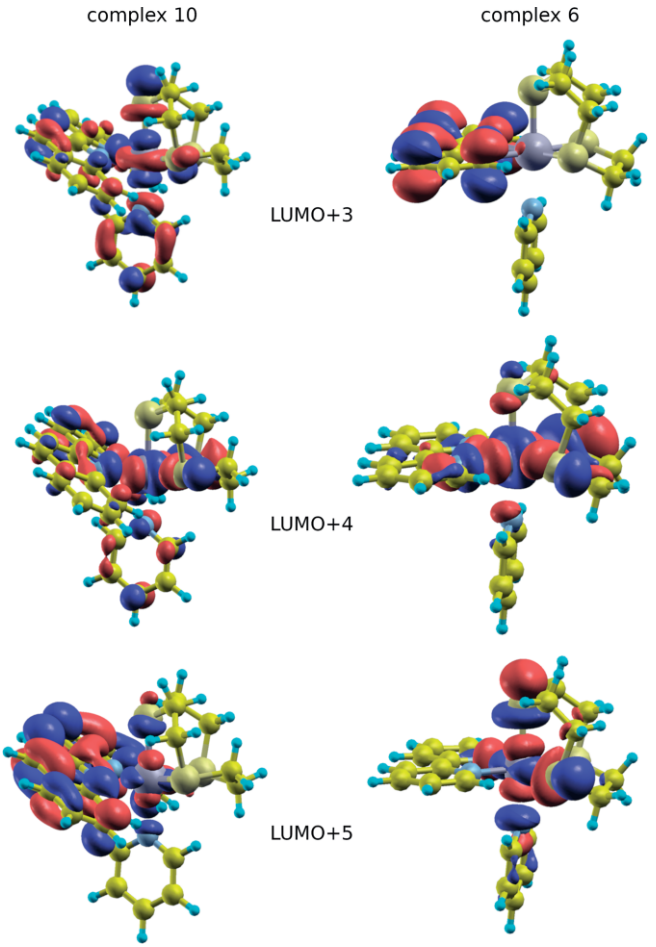

Figure 10. Selected virtual molecular orbitals for **6** (right) and **10** (left) in the singlet ground state.

The other significant photochemical difference between the two complexes concerns the photoinduced dissociation of the chelating diimine, that occurs in **10** (bq) but not in **6** (bpy). We observe that the binding of bq is arguably weaker than that of bpy because of its tilted coordination geometry that leads to a smaller overlap in the bonding orbitals.

In conclusion, contrary to what has been found by Turro and co-workers for *mer*-[Ru(tpy)(chel)(py)]$^{2+}$ species (chel = bpy or bq), where the distortions induced by the bulky bq led to an increased photoinduced release of py compared to bpy,[15] in our case – mainly because of the *facial*, rather than *meridional*, geometry of the complex – the distortions led to the preferential photo-dissociation of biquinoline itself.[38]

Although triplet states are generally thought to be responsible for the photochemistry of ruthenium complexes via facile intersystem crossing, we are confident that our analysis based on singlet ground and excited states captures the essential features of complex **10**. In fact, the previous work on complex **6** has shown that triplet excited states trace the character and ground state orbital composition of the singlet counterparts.[23]

3. Conclusions

The phototriggered release of pyridine from the series of water-soluble model complexes [Ru([9]aneS$_3$)(chel)(py)]Cl$_2$ was thoroughly investigated as a function of the nature of the chelating diimine {chel = 2,2′-bipyridine (bpy, **6**) 1,10-phenanthroline (phen, **7**), 4,7-diphenil-1,10-phenanthroline (Ph$_2$phen, **8**), dipyrido-[3,2-*a*:2′,3′-*c*]phenazine (dppz, **9**), 2,2′-biquinoline (brq, **10**)}. In **6**–**10**, owing to the face-capping 1,4,7-trithiacyclononane ligand ([9]aneS$_3$), the leaving ligand (py) and the diimine have a facial arrangement. Our aim is to establish whether this type of complexes might be realistically used in photoactivated chemotherapy (PACT) in the future.

We found that compounds **6**–**9** behave quite homogeneously, and their photochemical behavior is not particularly affected by the nature of the diimine: When irradiated with light at 470 nm, they rapidly and quantitatively release the coordinated pyridine, generating selectively the corresponding aqua species [Ru([9]aneS$_3$)(chel)(OH$_2$)]$^{2+}$ (**1aq**–**4aq**). Even though **6** was found to be non-phototoxic against the MDA-MB-231 human mammary carcinoma cells,[25] in the future we plan to investigate the phototoxicity also of **7**–**9**, as well as the $^1O_2$ production on selected compounds. The more lipophilic compounds in the series might be expected to have better accumulation in cancer cells and potentially show higher phototoxicity. We also argue that upon illumination the extended aromatic dppz ligand could generate singlet oxygen, thus giving to complex **9** two mechanisms of phototoxicity.

In addition, compounds **6**–**9** would be suitable for the photo-uncaging of many different pyridine-containing drugs, potentially for the treatment of both cancer and bacterial infections. This strategy does not require the concomitant formation of an active (e.g. cytotoxic) metal fragment. Some examples of py-containing drugs that have been coordinated to ruthenium previously (Figure 11) are the antibacterial isoniazid (**L1**),[39] the P-450 inhibitors metyrapone (**L2**) and abiraterone (**L3**),[21,40] and PARPs inhibitors [PARPs = poly(ADP-ribose) polymerase] such as nicotinamide (**L4**), quinazolin-4(3*H*)-one (**L5**), and 3-aza-5[H]-phenanthridin-6-one (**L6**).[41]

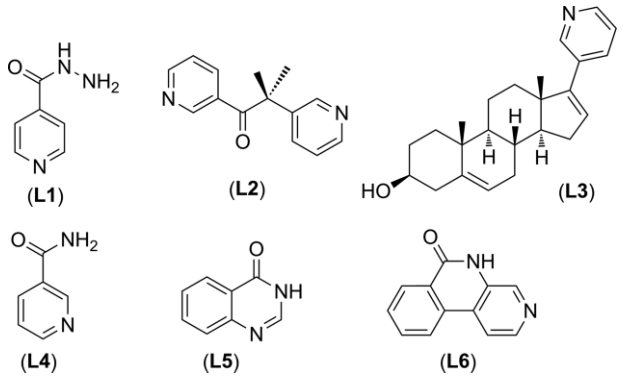

Figure 11. Examples of pyridine-containing drugs.

Complex **10** turned out to behave quite differently compared to the others in the series. As expected, the low-lying acceptor orbitals of bq induce a red-shift in the MLCT absorption maximum of the complex from ca. 430 to ca. 500 nm. However, contrary to the expectations, complex **10** turned out to be more photostable compared to **6**–**9** and – upon prolonged illumination with blue light – photo-dissociation of both py and bq, in nearly equal amounts, occurs. The single-crystal X-ray structure of **10** showed that in this complex, besides the expected distortion of coordinated bq due to its steric demand (a >35° tilt relative to the equatorial coordination plane), the orientation of py is nearly orthogonal compared to that found in **6** and **7**. A detailed theoretical investigation performed on **10** (and on **6** for comparison), showed that the biquinoline-induced geometrical distortions lead to differences in the nature of the excited states that might account for the different photochemical behavior of this complex.

In view of the potential investigation of these complexes as PACT agents, we observe that – unlike the rest of the series – upon irradiation with visible light complex **10** could generate in vivo a Ru^{II}-aqua species with two or even three coordination sites that is expected to be more reactive, and thus more cytotoxic, compared to the mono-aqua species generated from **6**–**9** (e.g. it might be capable of cross linking DNA). Consistent with this hypothesis, we found that the [Ru([9]aneS$_3$)(py)-(OH$_2$)$_2$]$^{2+}$ species binds rapidly the small amount of photo-released pyridine.

Finally, in the future it would be interesting to make the 6,6′-dimethyl-2,2′-bipyridine (dmbpy) analogue of these complexes. It might be expected to behave similarly to the bq complex and the photoreleased dmbpy could induce cell death according to what shown by Bonnet and co-workers.[22]

Experimental Section

Materials: All chemicals were purchased from Sigma–Aldrich and used as received. Solvents were of reagent grade. The ligand dppz (dipyrido-[3,2-*a*:2′,3′-*c*]phenazine) was prepared according to published procedures.[42] The precursors [Ru([9]aneS$_3$)Cl$_2$(dmso-S)] was synthesized as described in the literature.[28]

Instrumental Methods: Mono- and bi-dimensional (^{1}H-^{1}H COSY, ^{1}H-^{13}C HSQC) NMR spectra were recorded at room temperature with a Varian 400 or 500 spectrometer (^{1}H: 400 or 500 MHz, ^{13}C:100.5 or 125.7 MHz). ^{1}H and ^{13}C chemical shifts were referenced to the peak of residual non-deuterated solvent (δ = 7.26 and 77.16 for $CDCl_3$, 2.50 and 39.52 for [D_6]DMSO) or were measured relative to the internal standard DSS (δ = 0.00 ppm) for D_2O. Carbon resonances were assigned through the HSQC spectra; the resonances of quaternary carbon atoms were not assigned. ESI mass spectra were collected in the positive mode with a Perkin–Elmer APII spectrometer at 5600 eV. The UV/Vis spectra were obtained with an Agilent Cary 60 spectrophotometer, using 1.0 cm path-length quartz cuvettes (3.0 mL). A home-made LED apparatus,[43] a plastic-coated cylinder ($Ø_{max}$ = 20 mm, h = 110 mm), was used for performing the photochemical reactions in NMR or test tubes. The inside of the well features four pairs of juxtaposed LED stripes, containing five LEDs of the same color each (emission maxima: λ = 626, 590, 530, 470 nm; band width 10 nm, spectral range ca. 10 nm). LED stripes of the same color are located opposite to each other. One or more colors can be activated at the, with an emission power for each LED that can be regulated from 1 to 40 mW (30 mW for the green-emitting LEDs, λ = 530 nm).

Solid state infrared spectra were recorded with a Perkin–Elmer 983G spectrometer. Elemental analyses were performed in the Department of Chemistry of the University of Bologna (Italy).

X-ray Crystallography

Data collections were performed at the X-ray diffraction beamline (XRD1) of the Elettra Synchrotron of Trieste (Italy) equipped with a Pilatus 2 M image plate detector.

The collection temperature was 100 K (nitrogen stream supplied through an Oxford Cryostream 700); the wavelength of the monochromatic X-ray beam was 0.700 Å and the diffractograms were obtained with the rotating crystal method. The crystals were dipped in N-Paratone and mounted on the goniometer head with a nylon loop. The diffraction data were indexed, integrated and scaled using the XDS code.[44] The structures were solved by the dual space algorithm implemented in the SHELXT code.[45] Fourier analysis and refinement were performed by the full-matrix least-squares methods based on F2 implemented in SHELXL.[46] The Coot program was used for modeling.[47] Anisotropic thermal motion was allowed for all non-hydrogen atoms. Hydrogen atoms were placed at calculated positions with isotropic factors $U = 1.2 \times U_{eq}$, U_{eq} being the equivalent isotropic thermal factor of the bonded non-hydrogen atom. Crystallographic data and coordination distances and angles are in the Supporting Material.

CCDC 1588006 (for **7**), 1588009 (for **10**), 1588010 (for **11**), and 1588014 (for **12**) contain the supplementary crystallographic data for this paper. These data can be obtained free of charge from The Cambridge Crystallographic Data Centre.

Computational Methods: We performed periodic first principle calculations in the frame of density functional theory (DFT) with the Kohn–Sham orbitals expanded in a basis of plane waves and the effects of atomic core regions accounted for by pseudopotentials. The QUANTUM ESPRESSO suite of codes was used for all the computations.[48] To model an isolated molecule using a periodic code like QUANTUM ESPRESSO, a "molecule in the box" approach can be used: a single molecule is simulated in a unit cell large enough to minimize any interaction between the molecule itself and any of its periodic images. A cubic unit cell with edge length of 19.0 Å for complex **6** and 20.0 Å for complex **10** was found to give a minimum separation of 10 Å between nearest atoms of any two contiguous images. Both total energy and scf potential were corrected for the effect of the fictitious periodicity with the Martyna–Tuckerman method.[49] Ultrasoft pseudopotentials were used throughout the calculations.[50] The exchange–correlation part of the energy functional was modeled with the (spin-unpolarized) generalized gradient approximation (GGA), in the PBE parameterization.[51] The plane wave expansion of the crystalline orbitals was truncated at a cutoff energy of 340 eV and a corresponding tenfold cutoff was used for the expansion of the augmentation charge needed by the ultrasoft pseudopotential method. Integrals over the first Brillouin zone in reciprocal space were approximated by evaluations of the integrand functions at the gamma point. Convergence thresholds for geometry optimization were 1.4×10^{-4} eV for total energy and 2.6×10^{-2} eV/Å for the maximum force component acting on atoms; a threshold of 1.4×10^{-8} eV was imposed for self-consistency. Excited state calculations and UV/Vis spectra simulation were performed with time dependent DFT (TDDFT). The QUANTUM ESPRESSO suite offers two codes for this purpose. The "turbo_davidson" code implements an improved Davidson-like algorithm for the computation of individual excitations clustered around a target energy value, which, differently from the "conventional" Davidson algorithm, can be located anywhere in the spectrum. The "turbo_lanczos" program uses a so-called "pseudo-Hermitian" variant of the recursive Lanczos Scheme to evaluate the whole absorption spectrum in a given energy range using only the occupied states obtained in a previous self-consistent field calculation. Both codes rely upon the formulation of the TDDFT problem in terms of the linearized quantum Liouville equation and the details about the algorithms can be found in the original papers.[52,53] 60 trial vectors, a maximum of 200 basis vectors in the Davidson subspace and a convergence threshold of 1.0×10^{-4} for the squared modulus of the residue were used for the "turbo_davidson" runs; 5000 Lanczos iterations for each of the three directions of the full dynamical polarizability tensor were used in the UV/Vis spectrum simulation with the "turbo_lanczos" code.

Synthesis of the Complexes: The preparations were performed in light-protected glassware.

[Ru([9]aneS$_3$)(bpy)Cl]Cl (1): The complex was prepared according to a modified literature procedure.[23] [Ru([9]aneS$_3$)Cl$_2$(dmso-S)] (100 mg, 0.23 mmol) was partially dissolved in EtOH (15 mL). Two equivalents of bpy (72 mg, 0.46 mmol) were added, and the mixture was heated to reflux for 3 h. After 10 min of refluxing, the solution changed from yellow to orange. Precipitation of the product in pure form (according to ^{1}H NMR spectrum) from the concentrated solution (ca. 8 mL) occurred upon standing at room temp. It was removed by filtration, washed with a few mL of EtOH and diethyl ether, and dried in vacuo. Yield: 72 %. [$C_{16}H_{20}Cl_2N_2RuS_3$] (509.2): calcd. C 37.79, H 3.96, N 5.51; found C 37.68, H 4.05, N 5.60. ^{1}H NMR (D_2O): δ = 9.05 (d, 2 H, H6,6′), 8.47 (d, 2 H, H3,3′), 8.13 (t, 2 H, H4,4′), 7.62 (t, 2 H, H5,5′), 2.77 (m, 12 H, [9]aneS$_3$, partially overlapped with the corresponding resonances of **1$_{aq}$**) ppm. ESI mass spectrum: m/z = 473.0 (calcd. 473.1) $[M]^+$. UV/Vis (H_2O): λ_{max} (ε, L mol^{-1} cm^{-1}) = 361 (2359), 417 (4296) nm.

[Ru([9]aneS$_3$)(phen)Cl]Cl (2): Same procedure as for complex **1**, using the same amount of precursor and phen (83.5 mg, 2 equiv.). Also in this case, after 10 min of refluxing, the ethanol solution changed from yellow to orange. Yield: 70 %. $C_{18}H_{20}Cl_2N_2RuS_3$ (533.3): C 40.60, H 3.79, N 5.26; found C 40.52, H 3.68,N 5.18. ^{1}H NMR (D_2O): δ = 9.48 (d, 2 H, H2,9), 8.78 (t, 2 H, H4,7), 8. 22 (s, 2 H, H5,6), 8.02 (d, 2 H, H3,8), 2.73 ppm (m, 12 H, [9]aneS$_3$, partially overlapped with the corresponding resonances of **2$_{aq}$**). ^{1}H NMR ($CDCl_3$): δ = 9.36 (d, 2 H, H2,9), 8.49 (d, 2 H, H4,7), 8.05 (s, 2 H, H5,6),

7.87 (d, 2 H, H3,8), 2.97 (m, 12 H, [9]aneS$_3$) ppm. $^{13}C\{^1H\}$ NMR from HSQC ($CDCl_3$): δ = 152.2 (C2,9): δ = 136.3 (C4,7), 127.8 (C5,6), 126.0 (C3,8), 34.1 ([9]aneS$_3$) ppm. ESI mass spectrum: *m/z* = 497.0 (calcd. 497.1) $[M]^+$. UV/Vis (H_2O): λ_{max} (ε, L mol^{-1} cm^{-1}) = 369 (4711), 415 (4423) nm.

[Ru([9]aneS$_3$)(4,7-Ph$_2$phen)Cl]Cl (3): Same procedure as for complex **1**, using the same amount of precursor and 4,7-Ph$_2$phen (153.2 mg, 2 equiv.). In this case, after 10 minutes of refluxing, the ethanol solution changed from yellow to orange-brown. Yield: 75 %. $C_{30}H_{28}Cl_2N_2RuS_3$ (685.4): calcd. C 52.62, H 4.12, N 4.09; found C 52.73, H 4.20, N 4.17. ^1H NMR (D_2O): δ = 9.52 (d, 2 H, H2,9), 8.15 (s, 2 H, H5,6), 7.98 (d, 2 H, H3,8), 7.69 (br. s, 10 H, Ph), 2.92 (m, 12 H, [9]aneS$_3$, partially overlapped with the corresponding resonances of **3$_{aq}$**) ppm. ^1H NMR ($CDCl_3$): δ = 9.40 (d, 2 H, H2,9), 8.07 (s, 2 H, H5,6), 7.78 (d, 2 H, H3,8), 7.57 (m, 10 H, Ph), 3.03 (m, 12 H, [9]aneS$_3$) ppm. $^{13}C\{^1H\}$ NMR from HSQC ($CDCl_3$): δ 151.9 (C2,9), 129.2 (Ph), 124.0 (C5,6), 122.4 (C3,8), 35.0 ([9]aneS$_3$) ppm. ESI mass spectrum: *m/z* = 649.1 (calcd. 649.3) $[M]^+$. UV/Vis (H_2O): λ_{max} (ε, L mol^{-1} cm^{-1}) = 370 (6598), 408 (5786) nm.

[Ru([9]aneS$_3$)(dppz)Cl]Cl (4): Same procedure as for complex **1**, using the same amount of precursor and dppz (129.1 mg, 2 equiv.). In this case, after 10 min of refluxing, the ethanol solution changed from yellow to red. Yield: 71 %. $C_{24}H_{22}Cl_2N_4RuS_3$ (635.5): calcd. C 45.42, H 3.49, N 8.83; found C 45.50, H 3.58, N 8.91. ^1H NMR ($CDCl_3$): δ = 9.77 (d, 2 H, H2,2′), 9.42 (d, 2 H, H4,4′), 8.46 (d, 2 H, H5,5′), 8.08 (d, 2 H, H6,6′), 8.00 (t, 2 H, H3,3′), 3.01 (m, 12 H, [9]aneS$_3$) ppm. $^{13}C\{^1H\}$ NMR from HSQC ($CDCl_3$): δ = 153.6 (C4,4′), 134.3 (C2,2′), 131.3 (C6,6′), 130.6 (C5,5′), 126.3 (C3,3′), 33.2 ([9]aneS$_3$) ppm. ESI mass spectrum: *m/z* = 599.0 (calcd. 599.1) $[M]^+$. UV/Vis (H_2O): λ_{max} (ε, L mol^{-1} cm^{-1}) = 357 (6875), 423 (4750) nm.

[Ru([9]aneS$_3$)(bq)Cl]Cl (5): [Ru([9]aneS$_3$)Cl$_2$(dmso-S)] (50 mg, 0.12 mmol) was partially dissolved in EtOH (2 mL), and two equivalents of 2,2′-biquinoline (0.24 mmol, 60 mg) were added. The mixture was microwave-heated at 140 °C for 90 min. The white powder (unreacted bq) was removed by filtration. Evaporation of the solvent afforded a purple solid that was dissolved in water, which was filtered to remove the remaining traces of unreacted bq. The solution was rotary evaporated to dryness, and the solid (pure **5**, according to the ^1H NMR spectrum) was dried in vacuo. (Yield 51.1 mg, 66 %). $C_{24}H_{24}Cl_2N_2RuS_3$ (607.9): calcd. C 47.36, H 3.97, N 4.60; found C 47.28, H 3.88, N 4.51. ^1H NMR (D_2O): δ = 9.10 (d, 2 H, H8,8′), 7.95 (t, 2 H, H7,7′), 7.65 (d, 2 H, H4,4′), 7.73 (m, 4 H, H5,5′ + H6,6′), 7.49 (d, 2 H, H3,3′), 2.43 (m, 12 H, [9]aneS$_3$) ppm. $^{13}C\{^1H\}$ NMR from HSQC (D_2O): δ = 139.0 (C4,4′), 132.8 (C7,7′), 129.6 (C5,5′), 129.1 (C3,3′), 128.6 (C8,8′), 119.4 (C6,6′), 33.1 ([9]aneS$_3$) ppm. ESI mass spectrum: *m/z* = 573.1 (calcd. 573.2) $[M]^+$. UV/Vis (H_2O): λ_{max} (ε, L mol^{-1} cm^{-1}) = 356 (20106), 373 (19574), 515 (4787) nm.

[Ru([9]aneS$_3$)(bpy)(py)]Cl$_2$ (6): Complex **1** (60 mg, 0.13 mmol) was dissolved in H_2O (5 mL), and pyridine (50 µL, 0.6 mmol) was added. The solution was heated to reflux for 3 h, and then it was rotary evaporated to dryness. The obtained solid was sonicated with acetone (2 mL), then removed by filtration, washed with acetone and diethyl ether, and dried in vacuo. The product was obtained in pure form according to the ^1H NMR spectrum. Yield: 66 %. $C_{21}H_{25}Cl_2N_3RuS_3$ (588.2): calcd. C 42.93, H 4.29, N 7.15; found C 42.65, H 4.25, N 7.08. ^1H NMR (D_2O): δ = 9.23 (d, 2 H, H6,6′), 8.66 (d, 2 H, *o*-py), 8.38 (d, 2 H, H3,3′), 8.16 (t, 2 H, H4,4′), 7.77 (d, 3 H, *p*-py + H5,5′), 7.26 (t, 2 H, *m*-py), 2,90 (m, 12 H, [9]aneS$_3$) ppm. ESI mass spectrum: *m/z* = 473.0 (calcd. 473.1) $[M - py + Cl]^+$. UV/Vis (H_2O): λ_{max} (ε, L mol^{-1} cm^{-1}) = 401 (4666) nm.

[Ru([9]aneS$_3$)(phen)(py)]Cl$_2$ (7): Same procedure as for **6**, using complex **2** (69 mg, 0.13 mmol). The product was obtained in pure form according to the ^1H NMR spectrum. Yield: 87 %. $C_{23}H_{25}Cl_2N_3RuS_3$ (612.4): calcd. C 45.17, H 4.12, N 6.87; found C 45.25, H 4.20, N 6.98. ^1H NMR (D_2O): δ = 9.63 (d, 2 H, H2,9), 8.76 (d, 2 H, *o*-py), 8.72 (m, 2 H, H4,7), 8.15 (s, 2 H, H5,6), 8.11 (t, 2 H, H3,8), 7.71 (d, 1 H, *p*-py), 7.20 (t, 2 H, *m*-py), 3.01 (m, 12 H, [9]aneS$_3$) ppm. $^{13}C\{^1H\}$ NMR from HSQC (D_2O): δ = 153.3 (C2,9), 152.9 (*o*-py), 138.2 (C4,7), 138.5 (C3,8 + C5,6), 129.0 (*p*-py), 126.8 (*m*-py), 32.2 ([9]aneS$_3$) ppm. ESI mass spectrum: *m/z* = 497.0 (calcd. 497.1) $[M - py + Cl]^+$. UV/Vis (H_2O): λ_{max} (ε, L mol^{-1} cm^{-1}) = 353 (5153), 405 (4384) nm. X-ray quality crystals of **7** were obtained by slow diffusion of diethyl ether into an EtOH solution of the complex.

[Ru([9]aneS$_3$)(4,7-Ph$_2$phen)(py)]Cl$_2$ (8): Same procedure as for **6**, using complex **3** (89 mg, 0.13 mmol). The product was obtained in pure form according to the ^1H NMR spectrum. Yield: 84 %. $C_{35}H_{33}Cl_2N_3RuS_3$ (764.2): calcd. C 55.04, H 4.35, N 5.50; found C 55.11, H 4.44, N 5.61. ^1H NMR (D_2O): δ = 9.73 (d, 2 H, H2,9), 8.87 (d, 2 H, *o*-py), 8.09 (d, 2 H, H3,8), 7.81 (m, 3 H, H5,6 + *p*-py), 7.60 (m, 10 H, Ph), 7.34 (t, 2 H, *m*-py), 3.11 (m, 12 H, [9]aneS$_3$) ppm. $^{13}C\{^1H\}$ NMR from HSQC (D_2O): δ = 152.9 (C2,9), 151.9 (*o*-py), 125.1 (C5,6) 130.5 (C3,8 + *p*-py), 126.9 (Ph), 126.7 (*m*-py), 33.4 ([9]aneS$_3$) ppm. ESI mass spectrum: *m/z* = 649.1 (calcd. 649.3) $[M - py + Cl]^+$. UV/Vis (H_2O): λ_{max} (ε, L mol^{-1} cm^{-1}) = 467 (7800), 413 (6600) nm.

[Ru([9]aneS$_3$)(dppz)(py)]Cl$_2$ (9): Same procedure as for **6**, using complex **4** (82 mg, 0.13 mmol). The product was obtained in pure form according to the ^1H NMR spectrum. Yield: 65 %. $C_{29}H_{27}Cl_2N_5RuS_3$ (714.1): calcd. C 48.80, H 3.81, N 9.81; found C 48.72, H 3.71, N 9.73. ^1H NMR (D_2O): δ = 9.76 (d, 2 H, H2,2′), 9.03 (d, 2 H, *o*-py), 8.85 (s, 2 H, H4,4′), 8.11 (t, 2 H, H3,3′), 8.00 (t, 2 H, *p*-py), 7.59 (m, 6 H, H5,5′ + H6,6′ + *m*-py), 3.05 (m, 12 H, [9]aneS$_3$) ppm. $^{13}C\{^1H\}$ NMR from HSQC (D_2O): δ = 155.3 (C2,2′), 152.2 (*o*-py), 139.6 (C4), 133.3 (C3,3′), 133.2 (*p*-py), 128.1 (C5,5′ + C6,6′), 126.8 (*m*-py), 31.8 ([9]aneS$_3$) ppm. ESI mass spectrum: *m/z* = 599.0 (calcd. 599.1) $[M - py + Cl]^+$. UV/Vis (H_2O): λ_{max} (ε, L mol^{-1} cm^{-1}) = 355 (11882), 423 (4117) nm.

[Ru([9]aneS$_3$)(bq)(py)]Cl$_2$ (10): Same procedure as for **6**, using complex **5** (83 mg, 0.13 mmol). The product was obtained in pure form according to the ^1H NMR spectrum. Yield: 85 %. $C_{29}H_{27}Cl_2N_3RuS_3$ (688.87): calcd. C 50.65, H 4.25, N 6.11; found C 50.73, H 4.32, N 6.21. ^1H NMR (D_2O): δ = 8.79 (s, 4 H, H3,3′ + H4,4′), 8.32 (m, 4 H, H8,8′ + *o*-py), 8.17 (m, 2 H, H5,5′), 7.88 (m, 1 H, *p*-py), 7.80 (m, 4 H, H7,7′ + H6,6′), 7.28 (t, 2 H, *m*-py), 2.52 (m, 12 H, [9]aneS$_3$) ppm. $^{13}C\{^1H\}$ NMR from HSQC (D_2O): δ = 154.9 (*o*-py), 141.0 (C3,3′), 139.5 (*p*-py), 133.3 (C4,4′), 129.7 (C7,7′), 128.8 (C5,5′), 127.0 (*m*-py), 126.9 (C8,8′), 120.3 (C6,6′), 35.8 ([9]aneS$_3$) ppm. ESI mass spectrum: *m/z* = 573.1 (calcd. 573.2) $[M - py + Cl]^+$. UV/Vis (H_2O): λ_{max} (ε, L mol^{-1} cm^{-1}) = 359 (14161), 378 (16207), 466 (2854), 493 (3771) nm. X-ray quality crystals of **10** were obtained by slow diffusion of diethyl ether into an EtOH solution of the complex.

***trans,cis*-[Ru(bq)Cl$_2$(CO)$_2$] (11):** To *trans,cis,cis*-RuCl$_2$(CO)$_2$(dmso-O)$_2$ (60 mg, 0.16 mmol) dissolved in $CHCl_3$ (3 mL), was added 2,2′-biquinoline (1 equiv., 43.2 mg), and the mixture was sonicated for a few minutes until complete dissolution of the ligand (yellow solution). After 4 h, small red crystals began to form. The crystals were filtered after one day and washed with $CHCl_3$ and diethyl ether and dried in vacuo (Yield 57.1 mg, 75 %). $C_{20}H_{12}Cl_2N_2O_2Ru$ (484.83): calcd. C 49.60, H 2.50, N 5.78; found C 49.72, H 2.61, N 5.89. ^1H NMR ($CDCl_3$): δ = 9.25 (d, 2 H, H8,8′), 8.56 (d, 2 H, H3,3′), 8.35 (d, 2 H, H4,4′), 8.04 (t, 2 H, H7,7′), 7.98 (d, 2 H, H5,5′), 7.79 (t, 2 H, H6,6′) ppm. $^{13}C\{^1H\}$ NMR ($CDCl_3$): δ = 195.61 (CO), 141.24 (C3,3′), 133.29 (C7,7′), 129.65 (C8,8′), 129.51 (C6,6′), 129.35 (C5,5′), 119.37 (C4,4′) ppm. ESI mass spectrum: *m/z* = 448.6 (calcd. 448.8) $[M - Cl]^+$. Selected IR absorption (cm^{-1}): Nujol, 2051 (ν_{CO}, s), 1981 (ν_{CO}, s).

[Ru([9]aneS$_3$)(bq)(NH$_3$)]Cl$_2$ (12): [Ru([9]aneS$_3$)(bq)Cl]Cl (**5**) (20 mg, 0.033 mmol) was dissolved in H_2O (1 mL), a 25 % ammonia solution in water (45 µL, 0.42 mmol) was added, and the mixture was heated in the microwave at 110 °C for 150 min. Then the solvent was rotary evaporated completely and the resulting oil was crushed with $CHCl_3$ to obtain a dark red solid that was filtered, washed with $CHCl_3$ and diethyl ether, and dried in vacuo. According to the ^{1}H NMR spectrum, the product was pure **12**. X-ray quality crystals of **12** were obtained by slow diffusion of diethyl ether into a methanol solution of the complex. (Yield 14.4 mg, 70 %). $C_{24}H_{27}Cl_2N_3RuS_3$ (624.48): calcd. C 46.07, H 4.35, N 6.72; found C 45.99, H 4.28, N 6.63. ^{1}H NMR (D_2O): δ = 8.91 (d, 2 H, H8,8′), 8.65 (m, 4 H, H3,3′+H4,4′), 8.14 (s, 2 H, H5,5′), 8.06 (t, 2 H, H7,7′), 7.86 (t, 2 H, H6,6′), 3.53 (br. s, 3 H, NH_3), 2.63 (m, 12 H, [9]aneS$_3$) ppm. ^{13}C{^{1}H} NMR from HSQC (D_2O): δ = 134.6 (C3,3′), 131.2 (C7,7′), 129.3 (C5,5′), 129.2 (C6,6′), 126.8 (C8,8′), 120.11 (C4,4′), 33.2 ([9]aneS$_3$) ppm. ESI mass spectrum: *m/z* = 573.0 (calcd. 573.2) [M – NH_3 + Cl]$^+$.

[Ru([9]aneS$_3$)(py)$_2$Cl]Cl (13): [Ru([9]aneS$_3$)Cl$_2$(dmso-S)] (50 mg, 0.13 mmol) was partially dissolved in EtOH (10 mL), pyridine (36 µL, 0.52 mmol) was added, and the mixture was heated to reflux for 5 h. During the heating a clear yellow-orange solution was obtained, from which a yellow precipitate started to form. After cooling the mixture to room temp., the product was removed by filtration, washed with EtOH and diethyl ether, and dried in vacuo. (Yield 49.7 mg, 75 %). The product was pure **13** according to the ^{1}H NMR spectrum. $C_{16}H_{22}Cl_2N_2RuS_3$ (509.94): calcd. C 37.64, H 4.34, N 5.49; found C 37.78, H 4.44, N 5.58. ^{1}H NMR (D_2O): δ = 8.70 (d, 4 H, *o*-py), 7.87 (t, 2 H, *p*-py), 7.43 (t, 4 H, *m*-py), 2.41 (m, 12 H, [9]aneS$_3$ partially overlapped with the corresponding resonances of **13$_{aq}$**) ppm. ESI mass spectrum: *m/z* = 475.0 (calcd. 475.1) [M]$^+$.

Acknowledgments

Financial support from the University of Trieste (FRA2015, G. B. and E. A.), Fondazione Beneficentia Stiftung, and the Australian Research Council (DE13101650, A. R.) is gratefully acknowledged. We wish to thank BASF Italia Srl for a donation of hydrated ruthenium chloride.

Keywords: Ruthenium · Chelates · Photoactivated chemotherapy · N ligands · Photoinduced ligand release

[1] a) D. E. J. G. J. Dolmans, D. Fukumura, R. K. Jain, *Nat. Rev. Cancer* **2003**, *3*, 380–387; b) A. Juzeniene, Q. Peng, J. Moan, *Photochem. Photobiol. Sci.* **2007**, *6*, 1234–1245; c) T. Debele, S. Peng, H.-C. Tsai, *Int. J. Mol. Sci.* **2015**, *16*, 22094–22136.

[2] G. Mayer, A. Heckel, *Angew. Chem. Int. Ed.* **2006**, *45*, 4900–4921; *Angew. Chem.* **2006**, *118*, 5020.

[3] K. Szaciłowski, W. Macyk, A. Drzewiecka-Matuszek, M. Brindell, G. Stochel, *Chem. Rev.* **2005**, *105*, 2647–2694.

[4] a) N. J. Farrer, L. Salassa, P. J. Sadler, *Dalton Trans.* **2009**, 10690–10701; b) N. A. Smith, P. J. Sadler, *Phil. Trans. R. Soc. A* **2013**, *371*, 20120519.

[5] U. Schatzschneider, *Eur. J. Inorg. Chem.* **2010**, *2010*, 1451–1467.

[6] E. Ruggiero, S. Alonso-de Castro, A. Habtemariam, L. Salassa, *Struct. Bond.* **2014**, *165*, 69–108.

[7] J. D. Knoll, C. Turro, *Coord. Chem. Rev.* **2015**, *282–283*, 110–126.

[8] H. Yin, M. Stephenson, J. Gibson, E. Sampson, G. Shi, T. Sainuddin, S. Monro, S. A. McFarland, *Inorg. Chem.* **2014**, *53*, 4548–4559.

[9] C. Mari, V. Pierroz, S. Ferrari, G. Gasser, *Chem. Sci.* **2015**, *6*, 2660–2686.

[10] V. H. S. van Rixel, B. Siewert, S. L. Hopkins, S. H. C. Askes, A. Busemann, M. A. Sieglerb, S. Bonnet, *Chem. Sci.* **2016**, *7*, 4922–4929.

[11] M. Ethirajan, Y. Chen, P. Joshi, R. K. Pandey, *Chem. Soc. Rev.* **2011**, *40*, 340–362; A. B. Ormond, H. S. Freeman, *Materials* **2013**, *6*, 817–840.

[12] http://theralase.com/pressrelease/health-canada-approves-clinical-trial-application-anti-cancer-drug/. http://theralase.com/pressrelease/theralase-research-published-international-peer-reviewed-journal/.

[13] a) G. Shi, S. Monro, R. Hennigar, J. Colpitts, J. Fong, K. Kasimova, H. Yin, R. DeCoste, C. Spencer, L. Chamberlain, A. Mandel, L. Lilge, S. A. McFarland, *Coord. Chem. Rev.* **2015**, *282–283*, 127–138; b) J. Fong, K. Kasimova, Y. Arenas, P. Kaspler, S. Lazic, A. Mandel, L. Lilge, *Photochem. Photobiol. Sci.* **2015**, *14*, 2014–2023; c) P. Kaspler, S. Lazic, S. Forward, Y. Arenas, A. Mandela, L. Lilge, *Photochem. Photobiol. Sci.* **2016**, *15*, 481–495.

[14] a) B. S. Howerton, D. K. Heidary, E. C. Glazer, *J. Am. Chem. Soc.* **2012**, *134*, 8324–8327; b) E. Wachter, D. K. Heidary, B. S. Howerton, S. Parkin, E. C. Glazer, *Chem. Commun.* **2012**, *48*, 9649–9651; c) D. Havrylyuk, D. K. Heidary, L. Nease, S. Parkin, E. C. Glazer, *Eur. J. Inorg. Chem.* **2017**, *2017*, 1687–1694.

[15] J. D. Knoll, B. A. Albani, C. B. Durr, C. Turro, *J. Phys. Chem. A* **2014**, *118*, 10603–10610.

[16] a) S. Betanzos-Lara, L. Salassa, A. Habtemariam, P. J. Sadler, *Chem. Commun.* **2009**, 6622–6624; b) S. Betanzos-Lara, L. Salassa, A. Habtemariam, O. Novakova, A. M. Pizarro, G. J. Clarkson, B. Liskova, V. Brabec, P. J. Sadler, *Organometallics* **2012**, *31*, 3466–3479.

[17] a) M. A. Sgambellone, A. David, R. N. Garner, K. R. Dunbar, C. Turro, *J. Am. Chem. Soc.* **2013**, *135*, 11274–11282; b) Y. Chen, W. Lei, G. Jiang, Y. Hou, C. Li, B. Zhang, Q. Zhou, X. Wang, *Dalton Trans.* **2014**, *43*, 15375–15384; c) J. D. Knoll, B. A. Albani, C. Turro, *Acc. Chem. Res.* **2015**, *48*, 2280–2287; d) T. Sainuddin, M. Pinto, H. Yin, M. Hetu, J. Colpitts, S. A. McFarland, *J. Inorg. Biochem.* **2016**, *158*, 45–54.

[18] a) T. Joshi, V. Pierroz, C. Mari, L. Gemperle, S. Ferrari, G. Gasser, *Angew. Chem. Int. Ed.* **2014**, *53*, 2960–2963; *Angew. Chem.* **2014**, *126*, 3004; b) C. Mari, V. Pierroz, A. Leonidova, S. Ferrari, G. Gasser, *Eur. J. Inorg. Chem.* **2015**, *2015*, 3879–3891.

[19] a) A. N. Hidayatullah, E. Wachter, D. K. Heidary, S. Parkin, E. C. Glazer, *Inorg. Chem.* **2014**, *53*, 10030–10032; b) K. T. Hufziger, F. S. Thowfeik, D. J. Charboneau, I. Nieto, W. G. Dougherty, W. S. Kassel, T. J. Dudley, E. J. Merino, E. T. Papish, J. J. Paul, *J. Inorg. Biochem.* **2014**, *130*, 103–111.

[20] a) T. Respondek, R. N. Garner, M. K. Herroon, I. Podgorski, C. Turro, J. J. Kodanko, *J. Am. Chem. Soc.* **2011**, *133*, 17164–17167; b) R. Sharma, J. D. Knoll, P. D. Martin, I. Podgorski, C. Turro, J. J. Kodanko, *Inorg. Chem.* **2014**, *53*, 3272–3274; c) N. Karaoun, A. K. Renfrew, *Chem. Commun.* **2015**, *51*, 14038–14041; H. Chan, J. B. Ghrayche, J. Wei, A. Renfrew, *Eur. J. Inorg. Chem.* **2017**, *2017*, 1679–1686.

[21] A. Zamora, C. A. Denning, D. K. Heidary, E. Wachter, L. A. Nease, J. Ruiz, E. C. Glazer, *Dalton Trans.* **2017**, *46*, 2165–2173.

[22] J. A. Cuello-Garibo, M. S. Meijer, S. Bonnet, *Chem. Commun.* **2017**, *53*, 6768–6771.

[23] G. Ragazzon, I. Bratsos, E. Alessio, L. Salassa, A. Habtemariam, R. J. McQuitty, G. J. Clarkson, P. J. Sadler, *Inorg. Chim. Acta* **2012**, *393*, 230–238.

[24] The phototriggered ligand release is more efficient compared to the corresponding photoactivable organometallic compounds of the type [Ru(η^6-arene)(N-N)(py)][PF_6]$_2$ previously developed by Sadler and coworkers (ref.[16]).

[25] I. Finazzi, I. Bratsos, T. Gianferrara, A. Bergamo, N. Demitri, G. Balducci, E. Alessio, *Eur. J. Inorg. Chem.* **2013**, *2013*, 4743–4753.

[26] F. Barigelletti, A. Juris, V. Balzani, P. Belser, A. von Zelewsky, *Inorg. Chem.* **1983**, *22*, 3335–3339.

[27] E. Baranoff, J.-P. Collin, J. Furusho, Y. Furusho, A.-C. Laemmel, J.-P. Sauvage, *Inorg. Chem.* **2002**, *41*, 1215–1222.

[28] B. J. Goodfellow, V. Félix, S. M. D. Pacheco, J. P. de Jesus, M. G. B. Drew, *Polyhedron* **1997**, *16*, 393–401.

[29] J. Madureira, T. M. Santos, B. J. Goodfellow, M. Lucena, J. P. de Jesus, M. G. Santana-Marques, M. G. B. Drew, V. Félix, *J. Chem. Soc., Dalton Trans.* **2000**, 4422–4431.

[30] B. Machura, R. Kruszynski, *Polyhedron* **2007**, *26*, 3336–3342.

[31] a) J. A. G. Drake, D. W. Jones, *Org. Magn. Reson.* **1982**, *18*, 42–44; b) A. G. Osborne, R. Green, I. H. Sadler, D. Reed, *Magn. Reson. Chem.* **1989**, *27*, 4–12.

[32] S. A. Moya, J. Guerrero, R. Pastene, R. Schmidt, R. Sariego, R. Sartori, J. Sanz-Aparicio, I. Fonseca, M. Martinez-Ripoll, *Inorg. Chem.* **1994**, *33*, 2341–2346.

[33] R. Lalrempuia, M. R. Kollipara, *Polyhedron* **2003**, *22*, 3155–3160.

[34] P. Belser, A. von Zelewsky, *Helv. Chim. Acta* **1980**, *63*, 1675–1702.

[35] We found that in the ^{1}H NMR spectra of complexes **5**, **10**, and **12**, the chemical shifts of the bq protons are remarkably affected by the nature of the solvent (e.g. [D_6]DMSO vs. D_2O), even though the sequence order is maintained (Figure S9).

[36] J. A. Cuello-Garibo, E. Perez-Gallent, L. van der Boon, M. A. Siegler, S. Bonnet, *Inorg. Chem.* **2017**, *56*, 4818–4828.

[37] The calculated UV/Vis spectra of complexes **6** and **10** reproduce quite well the general spectral features, even though the absorption bands are red-shifted by ca. 60 nm compared to experimental spectra. Calculations were performed in the vacuo, and this might be one of the reasons for this general shift. Note that in ref.[23] the singlet excited state transitions for complex **6**, calculated with a different approach, had a numerically similar shift – but in the opposite direction – with respect to the experimental transitions.

[38] The photorelease of bq from **10** is not attributable to the longer irradiation times: it occurs (in low amounts) also for short irradiation times and increases with the irradiation time, i.e. it is not a photobleaching of the complex.

[39] N. A. Smith, P. Zhang, S. E. Greenough, M. D. Horbury, G. J. Clarkson, D. McFeely, A. Habtemariam, L. Salassa, V. G. Stavros, C. G. Dowson, P. J. Sadler, *Chem. Sci.* **2017**, *8*, 395–404.

[40] A. Zara, C. A. Denning, D. K. Heidary, E. Wachter, L. A. Nease, J. Ruiza, E. C. Glazer, *Dalton Trans.* **2017**, *46*, 2165–2173.

[41] Z. Wang, H. Qian, S.-M. Yiu, J. Sun, G. Zhu, *J. Inorg. Biochem.* **2014**, *131*, 47–55.

[42] J. E. Dickeson, L. A. Summers, *Aust. J. Chem.* **1970**, *23*, 1023–1027.

[43] F. Battistin, F. Scaletti, G. Balducci, S. Pillozzi, A. Arcangeli, L. Messori, E. Alessio, *J. Inorg. Biochem.* **2016**, *160*, 180–188.

[44] W. Kabsch, *Acta Crystallogr., Sect. D* **2010**, *66*, 125–132.

[45] G. M. Sheldrick, *Acta Crystallogr., Sect. A* **2015**, *71*, 3–8.

[46] G. M. Sheldrick, *Acta Crystallogr., Sect. A* **2008**, *64*, 112–122.

[47] P. Emsley, K. Cowtan, *Acta Crystallogr., Sect. D* **2004**, *60*, 2126–2132.

[48] P. Giannozzi, S. Baroni, N. Bonini, M. Calandra, R. Car, C. Cavazzoni, D. Ceresoli, G. L. Chiarotti, M. Cococcioni, I. Dabo, A. Dal Corso, S. Fabris, G. Fratesi, S. de Gironcoli, R. Gebauer, U. Gerstmann, C. Gougoussis, A. Kokalj, M. Lazzeri, L. Martin-Samos, N. Marzari, F. Mauri, R. Mazzarello, S. Paolini, A. Pasquarello, L. Paulatto, C. Sbraccia, S. Scandolo, G. Sclauzero, A. P. Seitsonen, A. Smogunov, P. Umari, R. M. Wentzcovitch, *J. Phys. Condens. Matter* **2009**, *21*, 395502 (http://arxiv.org/abs/0906.2569).

[49] G. J. Martyna, M. E. Tuckerman, *J. Chem. Phys.* **1999**, *110*, 2810–2821.

[50] D. Vanderbilt, *Phys. Rev. B* **1990**, *41*, 7892–7895.

[51] J. P. Perdew, K. Burke, M. Ernzerhof, *Phys. Rev. Lett.* **1996**, *77*, 3865–3868.

[52] O. B. Malcioglu, R. Gebauer, D. Rocca, S. Baroni, *Comput. Phys. Commun.* **2011**, *182*, 1744–1754.

[53] X. Ge, S. J. Binnie, D. Rocca, R. Gebauer, S. Baroni, *Comput. Phys. Commun.* **2014**, *185*, 2080–2089.